Asociación Argentina
de Mecánica Computacional

Mecánica Computacional Vol XXXIII, págs. 2677-2687 (artículo completo)
Graciela Bertolino, Mariano Cantero, Mario Storti y Federico Teruel (Eds.)
San Carlos de Bariloche, 23-26 Setiembre 2014

EFFECTS OF STENOTIC PLAQUES IN REALISTIC CAROTID ARTERY ANEURYSM MODELS: A CFD STUDY

Marcelo A. Castro [a, d], **Nora L. Peloc** [b], **Christopher M. Putman** [c], **Juan R. Cebral** [d]

[a] *CONICET, Grupo de Investigación y Desarrollo en Bioingeniería, Facultad Regional Buenos Aires, UTN, Medrano 951, Buenos Aires, Argentina, marcelo.a.castro@gmail.com, http://sites.google.com/site/marceloadriancastro*

[b] *Universidad Favaloro, Facultad de Ingeniería, Ciencias Exactas y Naturales, Solís 453, Buenos Aires, Argentina*

[c] *Department of Interventional Neuroradiology, Inova Fairfax Hospital, 3300 Gallows Rd., Falls Church, Virginia, USA*

[d] *Department of Computational and Data Sciences, George Mason University, 4400 University Blvd., Fairfax, Virginia, USA, jcebral@gmu.edu, http://cfd.gmu.edu/~jcebral*

Keywords: Cerebral aneurysms, Stenosis, Numerical simulations, Rotational angiography

Abstract. Cerebral aneurysms may rarely coexist with a proximal artery stenosis. In that small percent of patients, such coexistence poses a challenge for interventional neuroradiologists and neurosurgeons to make the best treatment decision. According to previous studies, the incidence of cerebral aneurysms in patients with internal carotid artery stenosis is not greater than 5%, where the aneurysm is usually incidentally detected, being 2% for aneurysms and stenoses in the same cerebral circulation. Those cases pose a difficult management decision for the physician. Case reports showed patients who died due to aneurysm rupture months after endarterectomy but before aneurysm clipping, while others did not show any change in the aneurysm after plaque removal, having optimum outcome after aneurysm coiling. The aim of this study is to investigate the intraaneurysmal hemodynamic changes before and after treatment of stenotic plaque. Virtually created moderate stenoses in vascular models of internal carotid artery aneurysm patients were considered in a number of cases reconstructed from three dimensional rotational angiography images. The strategy to create those plaques was based on parameters analyzed in a previous work where idealized models were considered, including relative distance and stenosis grade. Ipsilateral and contralateral plaques were modeled. Wall shear stress and velocity pattern were computed from finite element pulsatile blood flow simulations. The results may suggest that relative angular position may change the wall shear stress within the aneurysm sac.

Copyright © 2014 Asociación Argentina de Mecánica Computacional http://www.amcaonline.org.ar

1 INTRODUCTION

Carotid artery aneurysms distal to an atheromatous plaque are usually incidentally detected by angiography in patients with stenotic lesions. The management of carotid artery stenosis is well-established for symptomatic stenosis with area reduction indices above 69%. However, the optimal approach for lower grades remains uncertain (Wasserman et al., 2005). If the patient also presents a distal aneurysm, hemodynamics may be significantly affected after the removal of a high grade plaque regardless their relative distance (Adams, 1977; Cebral et al., 2011). However, for lower degrees stenoses the hemodynamics may still exhibit significant changes if the aneurysm is close to the stenotic lesion (Castro et al., 2013a). The incidence of this kind of concomitant pathologies is low, however, the mortality and morbidity rate associated to the rupture of a cerebral aneurysm is high (Castro, 2013b). According to previous studies, the incidence of cerebral aneurysms in patients with internal carotid artery stenosis is not greater than 5.4% (Pappada et al. 1997; Kappelle et al., 2000; Espinosa et al., 2009, Rouleau et al. 2009). However, that percentage was less than 2% when the aneurysm was located in the same arterial circulation (Rouleau et al., 2009). In those cases, the coexistence of both pathologies in the same circulation poses a challenge for interventional neuroradiologists and neurosurgeons to make the best treatment decision.

A case report describes the treatment option for a patient with a stenosis in the carotid artery located proximal to an unruptured aneurysm (14.0x8.0 mm.) at the ophthalmic artery bifurcation in the same vascular circulation. A stent was successfully deployed to remove the stenosis. A few months after the intervention, no change was observed in the aneurysm size and the aneurysm was successfully treated with a coil embolization procedure (Espinosa et al., 2009). Another case report showed that a patient with a stenosis in the carotid artery and an asymptomatic unruptured aneurysm (5.0x10.0 mm) in the same artery at the posterior communicating artery bifurcation underwent a successful endarterectomy. The aneurysm would have been treated a few months later however, the patient died after a subarachnoid hemorrhage five months after the endarterectomy, but before the aneurysm treatment. Autopsy revealed that the aneurysm had grown up to 14.0x10.0 mm. before rupture (Adams, 1977). Simultaneous interventions were also reported (Navaneethan et al., 2006). According to a previous study, all patients with severe stenoses (stenosis diameter reduction greater than 60%, which is equivalent to a stenosis area reduction greater than 84%) exhibited a flow reduction greater than 30% when compared to the contralateral circulation (Archie et al, 1982). Consequently, the intra-aneurysmal hemodynamics may significantly change depending on how the ipsilateral flow rate increases after intervention. A recent report showed cases where a stent used as flow-diverting devices to treat cerebral aneurysm removed a proximal stenosis resulting in an increase of the intra-aneurysmal pressure and a consequent bleeding (Cebral et al., 2011).

In this work we investigate the effects of a virtual stenotic plaque in the hemodynamics of an internal carotid artery aneurysm by means of image-based finite element blood flow realistic simulations. A methodology to create the same kind of plaques based on a number of parameters previously investigated (grade, relative lineal and angular position, etc.) was proposed and developed. The methodology was used to create ipsilateral and contralateral models, and the hemodynamics was analyzed in a selected case. The velocity patterns and the wall shear stress spatial and temporal distributions were investigated due to their associations to aneurysm growth and rupture reported in previous works (Castro et al., 2009; Cebral et al., 2010; Castro et al., 2011).

Copyright © 2014 Asociación Argentina de Mecánica Computacional http://www.amcaonline.org.ar

2 METHODS

2.1 Vascular modeling

Rotational cerebral angiography images are the preferred modality for reconstructing vascular models harboring aneurysms due to their highest spatial resolution and contrast. Rotational scans were obtained with an 8-second acquisition that consisted in 120 projections obtained during a 180° rotation, which were reconstructed into a 3D dataset of 128^3 voxels covering a field of view of 54.02 mm on a dedicated workstation. The voxel resolution was therefore 0.422 mm. These data were exported into a PC for mathematic vascular modeling using a previously presented methodology (Yim et al., 2002; Cebral et al., 2005; Castro et al., 2006; Castro et al., 2009). Patients with aneurysms in the internal carotid artery distal to a low curvature segment where the plaque might have developed were considered. Vascular model were reconstructed using deformable models (Castro et al., 2006). The geometric model was then used to generate high-quality volumetric finite element grids composed of tetrahedral elements with an advancing front technique (Löhner, 1996a; Löhner, 1996b; Löhner, 1997). Element size was adjusted in order to approximately maintain the same number of elements in the normal and stenotic arteries, resulting in meshes containing between 1 and 2 million tetrahedra.

In order to add both ipsilateral and contralateral proximal stenotic plaques proximal to the aneurysm vascular models, two diametrically opposed seeds were identified based on the location of the aneurysm neck. Assuming a cylindrical configuration, a cutplane perpendicular to the axis was considered in order to derive a relation between the grade of the stenosis (G), the fractional area affected by the lesion (K), and the fractional constant distance compared to the arterial radius that the plaque penetrates into the lumen (X) (see Figure 1). Those quantities are related by a simple quadratic equation for eccentric stenoses (1).

$$X^2 - 2X + (G/K) = 0 \tag{1}$$

Based on a previous study, 65% degree moderate virtual stenotic plaques were created with the maximum narrowing 0.6 cm proximal to the aneurysm (Castro et al., 2013a). That relation allowed to determining the number of neighboring element around the seed that would be chosen to be displaced a constant distance into the lumen. The affected area was later smoothed in order to eliminate any topological problems caused by the displacement of the element points where in real meshes far from ideal configurations (Figure 2).

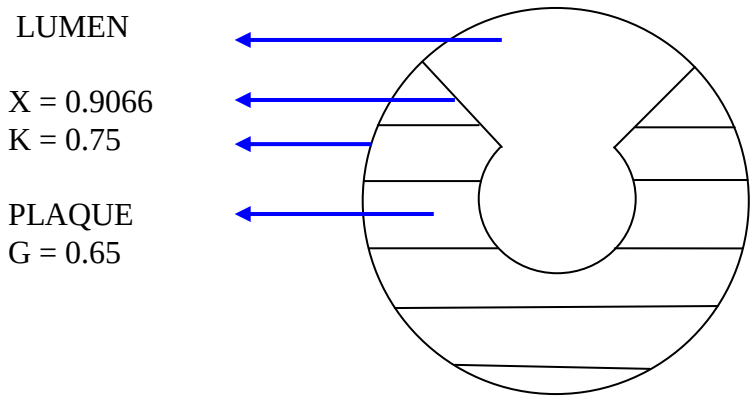

Figure 1. Schematic view of a cross-sectional area of a cylindrical vessel. From equation (1), X is derived for K=0.75 and G=0.65.

Copyright © 2014 Asociación Argentina de Mecánica Computacional http://www.amcaonline.org.ar

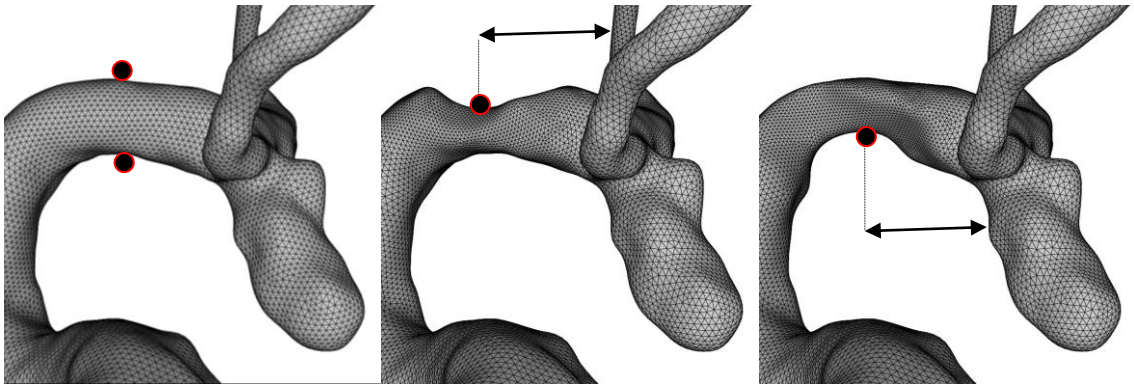

Figure 2. Locations of ipsilateral and contralateral seeds before and after the generation of the virtual proximal stenotic plaques for Case #7.

2.2 Computational hemodynamic modeling

Pulsatile finite element blood flow numerical simulations were performed for all models under the same flow conditions. Blood was modeled as an incompressible Newtonian fluid with density 1.0 g/cm^3 and viscosity 0.04 Poise. The governing equations were the unsteady Navier-Stokes equations in 3D (Mazumdar, 1982). Vessel walls were assumed as rigid, and no slip boundary conditions were applied at the walls. Pulsatile flow conditions, derived from phase-contrast magnetic resonance measurement in a healthy subject at the internal carotid artery, were imposed at the inlet of the models. Flow waveforms were scaled according to the inlet cross-sectional area in order to achieve a mean WSS of 15 dyn/cm^2 at the inflow boundary of each model. This choice is consistent with studies relating vessel area and flow rates in internal carotid and vertebral arteries (Cebral et al., 2008), as well as with the principle of minimal work expressed by Murray's law (Sherman, 1981). Fully developed pulsatile velocity profiles were prescribed with the use of the Womersley solution (Womersley, 1955; Taylor et al., 1998). Under the assumption that all distal vascular beds have similar total resistance to flow, traction-free boundary conditions with the same pressure level were applied at outlet boundaries. The Navier-Stokes equations were numerically integrated by using a fully implicit finite element formulation (Cebral et al., 2005). Our methodology is based on a projection scheme which arises from the hyperbolic character of the advection operator and the elliptic character of the pressure-Poisson equation. A fully implicit finite element formulation that yields to stable solutions for arbitrary time steps was utilized. The discretized momentum equation is solved using a generalized minimal residual (GMRES) algorithm, while the pressure equation, which is obtained by taking the divergence of the momentum and considering the incompressibility constraint, is solved using an incomplete lower-upper (ILU) preconditioned conjugate gradient solver. The algorithm is iterated to convergence in each time step. Two cardiac cycles were computed using 100 time-steps per cycle, and all of the reported results correspond to the second cardiac cycle.

2.3 Data analysis

Maps of WSS magnitude at the systolic peak were created to visualize the distribution of shear forces over selection regions on the aneurysm neck, an aneurysm bleb, and the aneurysm dome. In those regions, the lowest and highest WSS values are expected. Magnitude of the velocity and vector field was computed at a cut-plane at the systolic peak in order to identify differences in the flow patterns. At every time step, the magnitude of the WSS was computed for all the elements and averaged over each region.

Copyright © 2014 Asociación Argentina de Mecánica Computacional http://www.amcaonline.org.ar

3 RESULTS

In this study only moderate stenosis were considered (65% area reduction), therefore no inflow correction was included in the models after virtual intervention with respect to the original diseased arteries (Archie et al., 1982). The same flow rate wave form was applied to all models (Figure 3), which was acquired in a normal volunteer using phase-contrast magnetic resonance imaging (Cebral et al., 2003) and scaled in order to have a mean wall shear stress of 15 dyn/cm^2 (Cebral et al., 2008; Sherman et al., 1981), which corresponds to a Reynolds number close to 300. In order to scale the flow rate curve the Poiseuille flow equations were used to determine the relationship between the mean wall shear stress <*wss*>, the mean flow rate *Q*, the cross-sectional area *A*, and the blood viscosity μ (2).

$$\langle Q(A) \rangle = \frac{\langle wss \rangle}{4\mu\sqrt{\pi}} A^{3/2} \tag{2}$$

The criterion mentioned above is valid for a steady flow and is a good approximation to the pulsatile Womersley flow (Womersley, 1955).

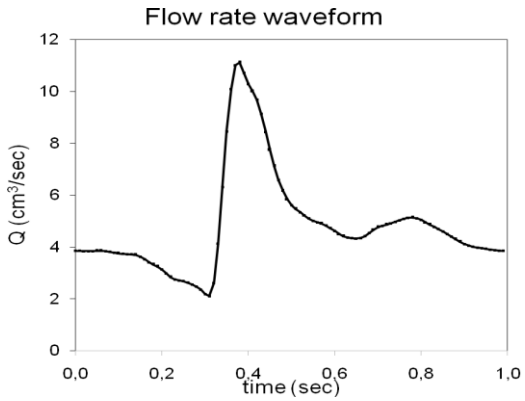

Figure 3. Flow rate waveform acquired from a normal volunteer using phase-contrast magnetic resonance imaging. Waveform is scaled according to the cross-sectional area in order to meet a mean wall shear stress of 15 dyn/cm^2.

The methodology described in the previous section was used to create the models containing a proximal ipsilateral plaque, and a proximal contralateral plaque from the original model without stenosis. The original (first column), contralateral (second column) and ipsilateral (third column) models are displayed in Figure 4 (cases #1, #2, and #3), Figure 5 (cases #4, #5, and #6), and Figure 6 (cases #7, #8, and #9).

A selected case (case #7) was randomly chosen to study the hemodynamic changes in the aneurysm due to the different configurations. Figure 7 shows the magnitude of the velocity field (top panel) and the vector field (bottom panel) at a cutplane within the aneurysm sac for the original (left), contralateral (middle), and ipsilateral (right) configurations at the systolic peak. The models with a proximal stenosis exhibit a velocity close to the aneurysm neck as much as twice as in the original model without plaque. Additionally, the original model has an intraaneurysmal vortex structure that qualitatively differs from that in the stenotic models (see Figure 7). Although differences between the ipsilateral and contralateral model can also be observed, they are less noticeable. Those differences arise from a different impaction zone, which is the result of the way in which each plaque deflects the main jet that emerges from the narrowed lumen.

Copyright © 2014 Asociación Argentina de Mecánica Computacional http://www.amcaonline.org.ar

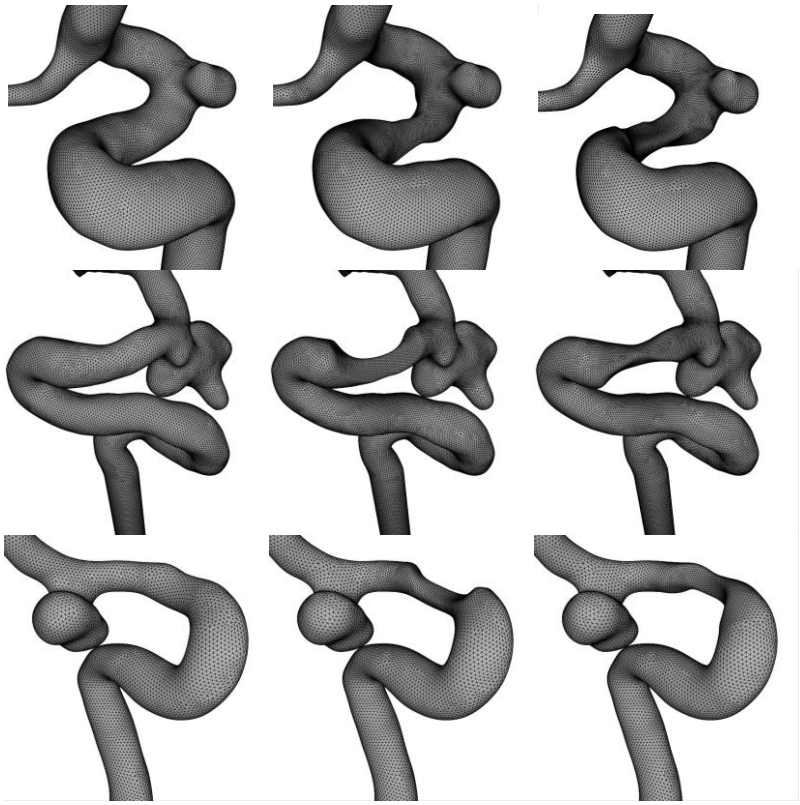

Figure 4**.**Vascular models for cases #1 (top row), #2 (middle row) and #3 (bottom row). Each column corresponds to the original aneurysm model (left), aneurysm model with a virtual proximal contralateral plaque (middle), and aneurysm model with a virtual proximal ipsilateral plaque (right).

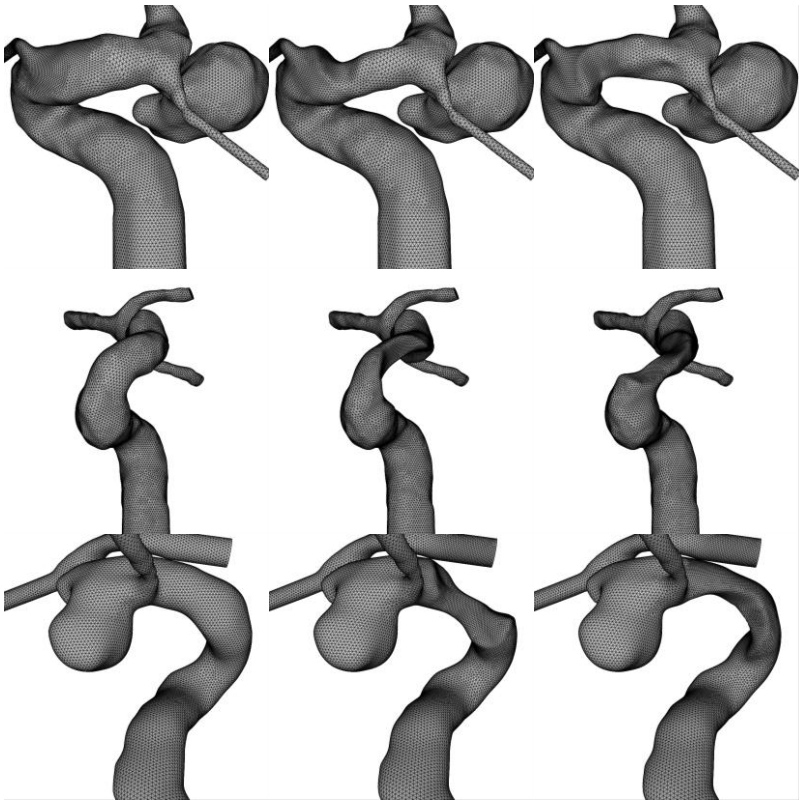

Figure 5**.**Vascular models for cases #4 (top row), #5 (middle row) and #6 (bottom row). Each column corresponds to the original aneurysm model (left), aneurysm model with a virtual proximal contralateral plaque (middle), and aneurysm model with a virtual proximal ipsilateral plaque (right).

Copyright © 2014 Asociación Argentina de Mecánica Computacional http://www.amcaonline.org.ar

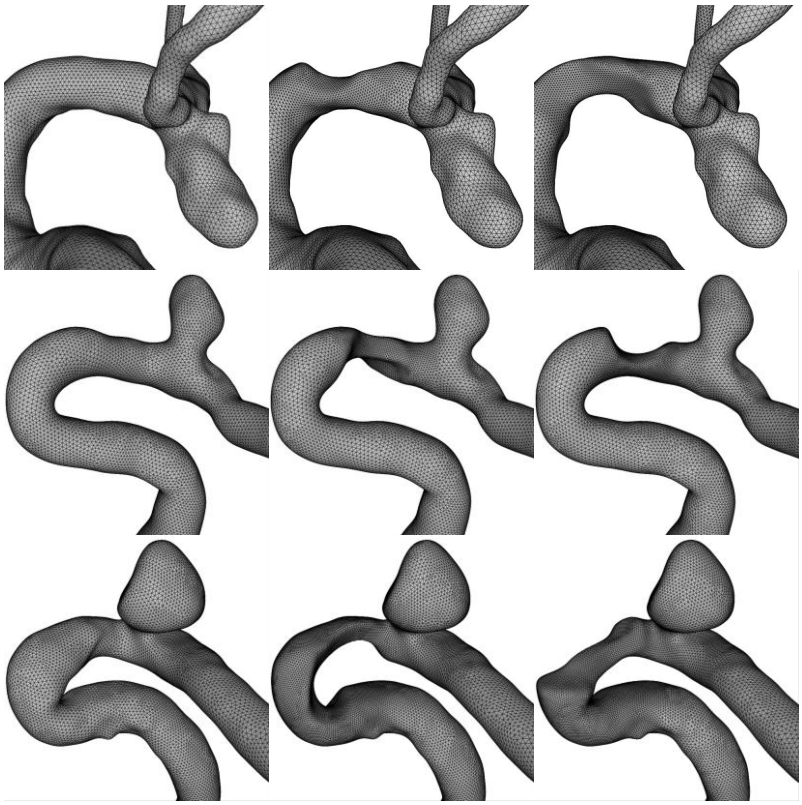

Figure 6**.**Vascular models for cases #7 (top row), #8 (middle row) and #9 (bottom row). Each column corresponds to the original aneurysm model (left), aneurysm model with a virtual proximal contralateral plaque (middle), and aneurysm model with a virtual proximal ipsilateral plaque (right).

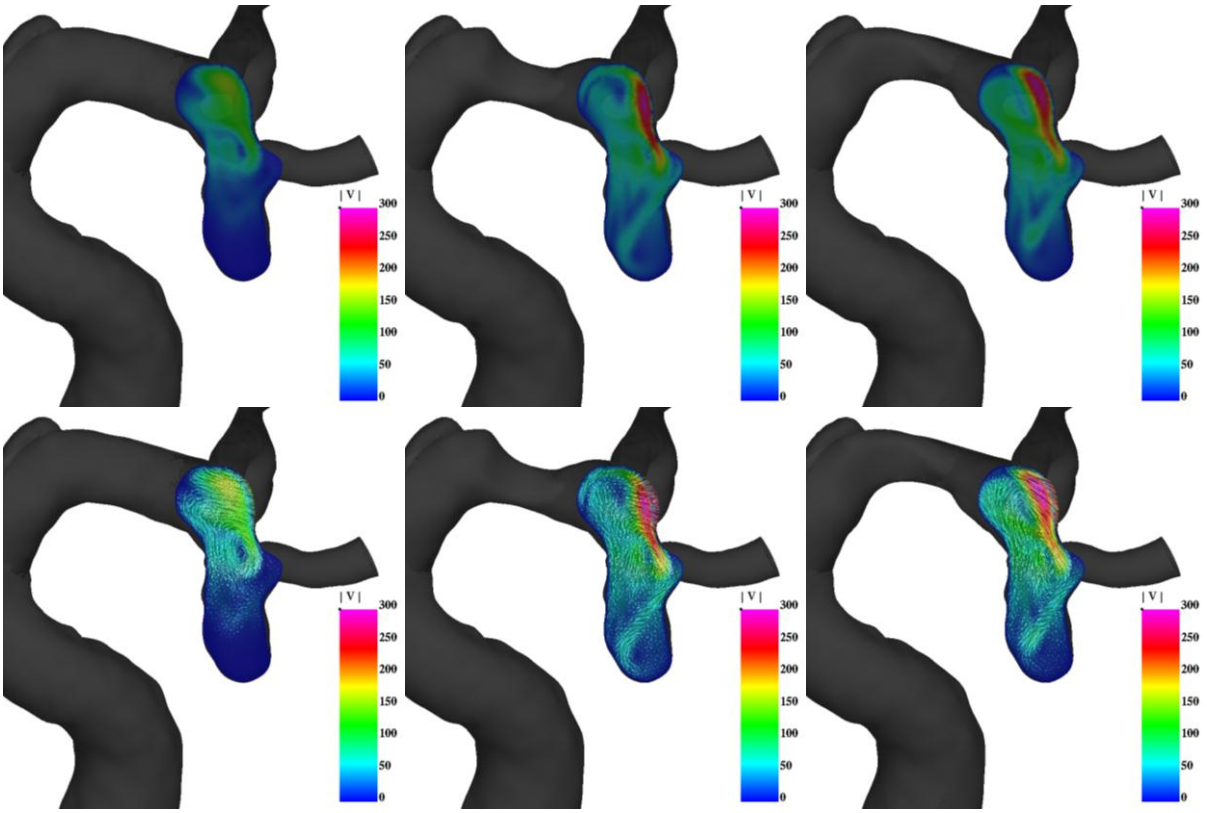

Figure 7**.** Magnitude of the velocity field (top panel) and the vector field (bottom panel) at a cutplane within the aneurysm sac for the original (left), contralateral (middle), and ipsilateral (right) configurations, at the systolic peak.

Copyright © 2014 Asociación Argentina de Mecánica Computacional http://www.amcaonline.org.ar

The wall shear stress distributions were compared at the systolic peak for the original, contralateral and ipsilateral models (Figure 8). A plaque close to the aneurysm causes an increased shear stress in the region of the wall opposed to the plaque, which affects the shear forces exerted over the aneurysm neck. The relocation of the impaction zone also produces higher penetration inside the sac. Consequently, the aneurysm bleb and the aneurysm dome are under a higher WSS in the contralateral model (Figure 8-middle). In order to investigate how those differences vary on time, the WSS was averaged over three selected regions: neck, bleb and dome, and the time evolution of the WSS was tracked in one cardiac cycle (Figure 9). The contralateral model is under higher WSS with respect to the ipsilateral model during the whole cycle at all regions. Compared to the models with a proximal stenotic plaque, the original model exhibits significantly lower WSS values at all time in all regions. At the aneurysm neck the maximum WSS in the contralateral configuration is 524.7 dyne/cm^2, compared to 401.3 dyne/cm^2 and 221.9 dyne/cm^2 for the ipsilateral and original configurations, respectively. For the bleb, which is under low WSS only in the original configuration, those values are 224.3 dyne/cm^2, 169.7 dyne/cm^2, and 104.0 dyne/cm^2 (contralateral, ipsilateral and original configurations). In the dome, the WSS drops to 76.5 dyne/cm^2, 70.6 dyne/cm^2, and 39.0 dyne/cm^2, for the contralateral, ipsilateral, and original configurations, respectively. The results are summarized in Table 1.

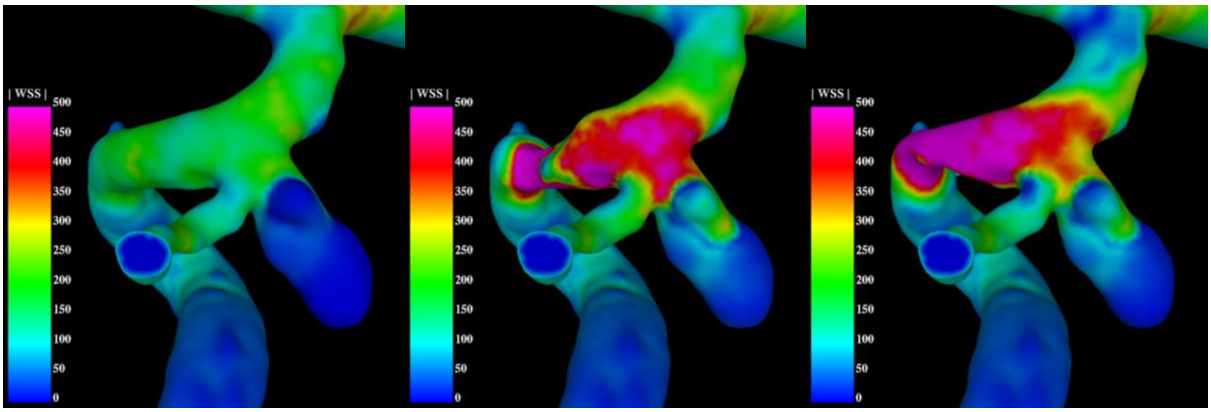

Figure 8. Wall shear stress distributions at the systolic peak for the original (left), contralateral (middle), and ipsilateral (right) models for case #7.

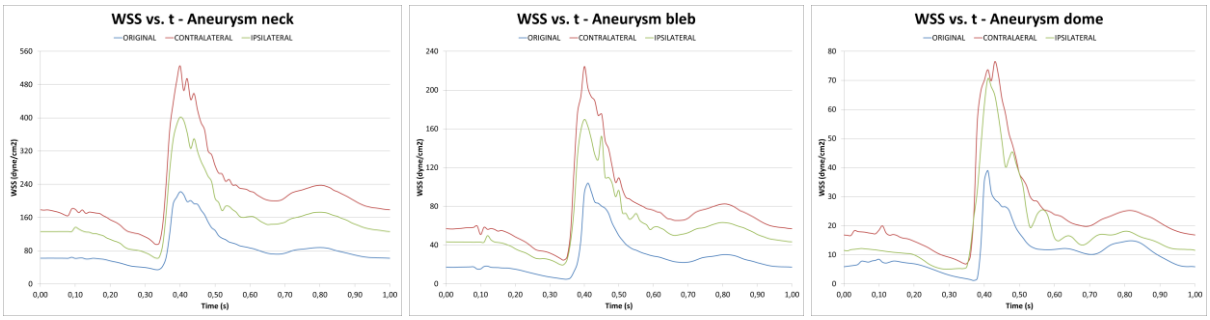

Figure 2. WSS at the aneurysm neck (left), aneurysm bleb (middle), and aneurysm dome (right), for the contralateral (red), ipsilateral (green), and original (blue) configurations along a cardiac cycle.

	Aneurysm NECK WSS (dyne/cm^2)			Aneurysm BLEB WSS (dyne/cm^2)			Aneurysm DOME WSS (dyne/cm^2)		
	ORIGINAL	**CONTRA**	**IPSI**	**ORIGINAL**	**CONTRA**	**IPSI**	**ORIGINAL**	**CONTRA**	**IPSI**
MIN	34.5	**95.3**	62.4	4.9	**24.6**	19.9	1.2	**7.0**	5.1
AVE	84.2	**220.4**	160.8	27.2	**75.8**	58.8	10.8	**24.5**	18.4
MAX	221.9	**524.7**	401.3	104.0	**224.3**	169.7	39.0	**76.5**	70.6

Table 1. Minimum, time-averaged and maximum WSS at the selected regions: neck, bleb and dome. The contralateral configuration in under the higher shear forces in all regions, while the original configuration without plaque exhibits the least forces.

Copyright © 2014 Asociación Argentina de Mecánica Computacional http://www.amcaonline.org.ar

4 DISCUSION

The aim of this preliminary work is to investigate the main characteristics of the intra-aneurysmal hemodynamics affected by a proximal artery stenosis, and the expected changes after a plaque removal. For that purpose, we present a methodology to create virtual eccentric proximal stenotic plaques to a cerebral aneurysm in the upper internal carotid artery, and applied a previous developed methodology for patient-specific image-based computational hemodynamics studies of vascular cerebral networks harboring intracranial aneurysms (Taylor et al., 1998; Yim et al., 2002; Cebral et al., 2005; Castro et al., 2009) to study the intra-aneurysmal hemodynamics in a selected patient. Vascular models with virtual stenotic plaques were successfully created. The methodology presented is suitable for the creation of different kind of plaques based on three parameters. Moderate eccentric stenoses with a 65% reduction in area were generated in two different angular locations: contralateral and ipsilateral to the aneurysm neck, and a moderate stenosis close to the aneurysm. It was observed that the contralateral configuration deflect the main jet toward the aneurysm neck producing higher WSS values within the aneurysm sac at each time step. Systematically, the contralateral configuration produced shear forces more than twice than the original model without plaque. Due to the deflection of the jet, that increase in the forces were not so pronounced in the ipsilateral case. However, they still were far above those observed in the original model. Therefore, the removal of the plaque produce a change in the force exerted by the flow over the aneurysm endothelial cells, which in the analyzed case depends on geometrical parameters. Assessing the clinical implications of those changes is beyond the scope of this work. While some authors have suggested that low wall shear stress triggers biological mechanisms that may results in aneurysm wall weakening and rupture (Xiang et al., 2011), others have shown that sudden increment in the intra-aneurysm flow, wall shear stress, and pressure are responsible for that outcome (Cebral et al., 2011).

The methodology has some limitations. The study only included low and mild stenoses. Severe stenosis would require higher resolution models to correctly depict transition to turbulence and also to consider flow correction after the intervention. However, different turbulent models lead to different results (Patel et al., 1984; Stroud et al., 2002; Varghese et al., 2003; Varghese et al., 2007; Castro et al., 2013a). For comparability purposes aiming to establishing the configuration with higher rupture risk, the laminar flow is an acceptable assumption. The study did not assume that the flow rate changed after the elimination of the plaque. It is worth mentioning that current evidence show that this phenomenon occurs for much higher grades (above 80% reduction in area). Although the correct vascular geometry reconstruction results in realistic blood flow simulations (Cebral et al., 2007), the use of non-patient-specific flow rate waveforms imposed at the inlet of our models may incorporate some errors. This limitation, which is suffered by most similar CFD studies, is partially overcome by wall shear stress normalization at inflow segments, which allows comparison between different models. Other model assumptions had limited impact on intra-aneurysmal hemodynamic characterization, as it was shown in a previous work (Rouleau et al., 2009; Cebral et al., 2005).

Future works will include a statistical analysis over all cases, the inclusion of different configurations, and the analysis of patient-specific models concomitant pathologies. Those results will serve to test different theories and potentially contribute to better clinical recommendations.

Copyright © 2014 Asociación Argentina de Mecánica Computacional http://www.amcaonline.org.ar

5 ACKNOWLEDGEMENTS

Marcelo Castro wants to acknowledge CONICET (Consejo Nacional de Investigaciones Científicas y Técnicas, Argentina) for financial support (PIP CONICET 2011-2013 Nr. 287), and ANPCyT (Agencia Nacional de Promoción Cinetífica y Tecnológica, Argentina).

REFERENCES

Adams, H.P., Carotid stenosis and coexisting ipsilateral intracranial aneurysm: a problem in management, *Arch Neurol*, 34, 515-516, 1977.

Archie, J.P., Feldtman, R.W., Collateral cerebral vascular resistance in patients with significant carotid stenosis, *Stroke*, 13(6):829–831, 1982.

Castro, M.A., Putman, C.M., Cebral, J.R., Patient-specific computational modeling of cerebral aneurysms with multiple avenues of flow from 3D rotational angiography images, *Acad Radiol*, 13, 811–821, 2006.

Castro, M.A., Putman, C.M., Cebral, J.R., Hemodynamic Patterns of Anterior Communicating Artery Aneurysms: A Possible Association with Rupture, *Am J Neurorad*, 30(2), 297-302, 2009.

Castro, M.A., Putman, C.M., Cebral, J.R., Computational analysis of anterior communicating artery aneurysm shear stress before and after aneurysm formation, *J Phys Conf Ser*, 332, 1-7, 2011.

Castro, M.A., Peloc, N.L., Putman, C.M., Cebral, J.R., Cerebrovascular systems with concomitant pathologies: A computational hemodynamics study, *J Phys Conf Ser*, 447, 1–10, 2013a.

Castro, MA, Understanding the role of hemodynamics in the initiation, progression, rupture, and treatment outcome of cerebral aneurysms from medical image-based computational studies, *ISRN Radiology*, 2013, 1-17, 2013b.

Cebral, J.R., Castro M.A., Burgess, J., Putman, C.M., Blood flow models of the circle of Willis from magnetic resonance data, *J Eng Math*, 47(3/4):369–386, 2003.

Cebral. J.R., Castro, M.A., Appanaboyina, S., Putman, C., Millán, D., Frangi, A., Efficient Pipeline for Image-Based Patient-Specific Analysis of Cerebral Aneurysms Hemodynamics: Technique and Sensitivity, *IEEE - Trans Med Imag - Special Issue on Vascular Imaging*, 24(4), 457-467, 2005.

Cebral, J.R., Pergolizzi, R.S., Putman, C.M., Computational fluid dynamics modeling of intracranial aneurysms: Quantitative comparison with cerebral angiography, *Acad Radiol*, 14, 804-813, 2007.

Cebral, J.R., Castro, M.A., Putman, C.M., Alperin, N., Flow-area relationship in internal carotid and vertebral arteries, *Physiol Meas*, 29(10), 585-594, 2008.

Cebral, J.R., Sheridan, M., Putman, C.M., Hemodynamics and bleb formation in intracranial aneurysms, *Am J neuroradiol*, 31, 304-310, 2010.

Cebral, J.R., Mut, F., Raschi, M., Scrivano, E., Ceratto, R., Lylyk, P., Putman, C.M., Aneurysm rupture following treatment with flow-diverting stents: Computational hemodynamics analysis of treatment, Am J Neurorad, 32:27–33, 2011.

Espinosa, G., Dzieciuchowicz, L., Grochowicz, L., Endovascular treatment of carotid stenosis associated with incidental intracranial aneurysm, *Ann Vasc Surg*, 23, 688.e1-688.e5, 2009.

Kappelle, L.J., Eliasziw, M., Fox, A.J., et al., Small unruptured intracranial aneurysm and management of symptomatic carotid artery stenosis: North American symptomatic carotid endarterectomy trial group, *Neurology*, 55, 307–309, 2000.

Löhner, R., Extensions and improvements of the advancing front grid generation technique, *Comp Meth Appl Mech Eng*, 5, 119–132, 1996a.

Löhner, R., Regridding surface triangulations, *J Comp Phys*, 126, 1–10, 1996b.

Löhner, R., Automatic unstructured grid generators, *Finite Elements Analysis Design*, 25, 111–134, 1997.

Mazumdar, J.N., Biofluid Mechanics, World Scientific, Singapore, 41-104, 1992.

Copyright © 2014 Asociación Argentina de Mecánica Computacional http://www.amcaonline.org.ar

Navaneethan, S.D., Kanna, V.S., Osowo, A., Shrivastava, R., Singh, S., Concomitant intracranial aneurysm and carotid artery stenosis: A therapeutic dilemma, *Sothern Medical Journal*, 99(7), 757-758, 2006.

Pappada, G., Fiori, L., Marina, R., et al., Incidence of asymptomatic of asymptomatic berry aneurysms among patients undergoing carotid artery endarterectomy, *J Neurosurg Sci*, 41, 257-262, 1997.

Patel, V.C., Rodi, W., Scheuerer, G., Turbulence models for near-wall and low Reynolds number flows : A review, *AIAA J*, 22, 1308-1319, 1984.

Rouleau, P.A., Huston, J., Gilbertson, J., Brown, R.D., Meyer, F.B., Bower, T.C., Carotid Artery Tandem Lesions: Frequency of Angiographic Detection and Consequences for Endarterectomy, *Am J Neuroradiol*, 20, 621-625, 2009.

Sherman, T. F., On connecting large vessels to small. The meaning of Murray's law, *J Gen Physiol*, 78, 431–453, 1981.

Stroud, J.S., Berger, S.A., Saloner, D., Numerical analysis of flow through a severely stenotic carotid artery bifurcation, *J Biomecch Eng*, 124, 9-20, 2002.

Taubin, G., A signal processing approach to fair surface design, *Proc. 22nd Ann Conf Computer Graphics and Interactive Techniques (SIGGRAPH 1995)*, 351-358, 1995.

Taylor, C.A., Hughes, T.J.R., Zarins, C.K., Finite element modeling of blood flow in arteries, *Comp Meth Appl Mech Engin*, 158, 155–196, 1998.

Varghese, S.S., Frankel, S.H., Numerical modelling of pulsatile turbulent flow in stenotic vessels, *J Biomech Eng*, 125, 445–460, 2003.

Varghese, S.S., Frankel, S.H., Fischer, P.F., Direct numerical simulation of stenotic flows, *J Fluid Mech*, 582, 253-280, 2007.

Wasserman, B.A., Wityk, R.J., Trout, H.H., Virmani, R., Low-grade carotid stenosis: Looking beyond the lumen with MRI, *Stroke*, 36:2504–2513, 2005.

Womersley, J.R., Method for the calculation of velocity, rate of flow and viscous drag in arteries when the pressure gradient is known, *J Physiol*, 127, 553–563, 1955.

Xiang, J., Tremmel, M., Kolega, J., Levy, E., Natarajan, S., Meng, H., Newtonian viscosity model could overestimate wall shear stress in intracranial aneurysm domes and underestimated rupture risk, *J Neurointerv Surg*, 4(5), 351–357, 2011.

Yim, P.J., Vasbinder, B., Ho, V.H., et al., A deformable isosurface and vascular applications, *Proc SPIE*, 4684, 1390–1397, 2002.

Copyright © 2014 Asociación Argentina de Mecánica Computacional http://www.amcaonline.org.ar